

Ab Initio Molecular Dynamics Simulations of the Infrared Spectra of H_3O_2^- and D_3O_2^-

Martina Kaledin,* John M. Moffitt,[†] Craig R. Clark,[‡] and Fareeha Rizvi

Chemistry and Biochemistry, Kennesaw State University, 1000 Chastain Rd.,
Box 1203, Kennesaw, Georgia 30144

Received November 24, 2008

Abstract: We present the infrared spectra of H_3O_2^- and D_3O_2^- calculated using MP2 direct molecular dynamics approach at temperatures of 100 and 300 K. The spectral peaks were assigned using the normal-mode analysis, instantaneous normal-mode analysis, isotopic substitution, polarized infrared absorptions, and analysis of the position–position correlation function. Our results predict the bridging hydrogen stretch between 600 and 900 cm^{-1} and bridging hydrogen bend vibrations between 1250 and 1650 cm^{-1} . We also examine two DFT methods (B3PW91 and B3LYP) and report on the differences between them and the MP2 spectra.

1. Introduction

Proton transfer in biological systems is thought to often proceed through hydrogen-bonded chains of water molecules.¹ Such chains could act as proton wires by providing an effective pathway for the rapid translocation of protons over long distances. A characterization of proton wires at the microscopic level is required for a better understanding of complex systems. The hydrated hydroxide ion, H_3O_2^- is one of two fundamental structures (i.e., H_3O_2^- and H_5O_2^+) involved in the proton transfer. The bridging proton in H_3O_2^- and H_5O_2^+ is located between two oxygen atoms, e.g. $[\text{HO}-\text{H}-\text{OH}]^-$ and $[\text{H}_2\text{O}-\text{H}-\text{OH}_2]^+$. The structure and dynamics of H_3O_2^- have been the subject of several theoretical studies.^{2–18} The geometry of H_3O_2^- has been predicted to be asymmetric with a longer H-bond of 1.342 Å and a shorter one of 1.125 Å.¹¹ In H_3O_2^- two equivalent equilibrium structures of C_1 symmetry are separated by a transition structure of C_2 symmetry that comprises a low barrier^{2,11} to proton transfer between two OH^- fragments. Parrinello et al.³ investigated the quantum character of the

shared proton in H_3O_2^- and H_5O_2^+ system using ab initio techniques. These calculations at room temperature have shown that the shared proton in the strongly hydrogen bonded H_5O_2^+ behaved in an essentially classical manner, while in the H_3O_2^- complex, quantum effects played a crucial role even at room temperature. Iyengar et al.¹⁷ studied the properties of larger OH^- water cluster $\text{OH}^-(\text{H}_2\text{O})_6$ that displays a hydroxide ion migration mechanism. Recently, Yang and Kuhn¹⁸ investigated the effect of deuteration of the hydrated hydroxide ion using a quantum dynamical model and found zero-point energies in quantitative agreement with diffusion Monte Carlo calculations.

There has been progress in the experimental investigations of H_3O_2^- and H_5O_2^+ .^{6–16,19–22} Price et al. reported the argon predissociation IR spectrum of H_3O_2^- in the OH stretching region¹⁹ and observed a strong sharp feature at 3653 cm^{-1} , which lies above vibrational band corresponding to the free hydroxide anion and below the region associated with the free OH stretch. Two weaker bands centered near 3100 and 3380 cm^{-1} were assigned to ionic bridging hydrogen vibration that is mixed with the H_2O bending mode. Another experimental study analyzed the hydration of the OH^- anion.²⁰ The vibrational spectra of cold hydrated ions $\text{OH}^-(\text{H}_2\text{O})_{1–3}$ display a sharp feature in the OH stretching region, and in larger clusters a new feature appears in the region associated with interwater hydrogen bonding. A set of argon predissociation spectra for H_3O_2^- and H_5O_2^+ were reported by Johnson's group.²¹ Recent VSCF/CI¹⁴ and

* Corresponding author phone: +1-770-423-6281; fax: +1-770-423-6744; e-mail: mkaledin@kennesaw.edu.

[†] Present address: University of Connecticut, Department of Molecular and Cell Biology, Storrs, CT 06269. E-mail: john.moffitt@uconn.edu.

[‡] Present address: Georgia Institute of Technology, Department of Chemistry and Biochemistry, Atlanta, GA 30332. E-mail: craig.clark@gatech.edu.

diffusion Monte Carlo^{16,21} calculations for H_3O_2^- indicate that the lowest-energy excitation involving displacement of the proton along the O–O axis would occur with much lower energies (650–720 cm^{-1}) than those predicted by standard normal-mode analysis at the global minimum.²

Motivated by uncertainties in theoretical and experimental predictions of bridging hydrogen vibrations, we recently reported the vibrational analysis of the H_5O_2^+ IR spectrum in the range 600 and 1900 cm^{-1} .²³ We presented calculations of the IR spectrum of H_5O_2^+ using the driven molecular dynamics (DMD) method and assigned the dominant spectral features near 1000 and 1780 cm^{-1} to the proton transfer coupled to the torsion motion and to the H_2O monomer bend coupled with proton transfer, respectively.

High level theoretical simulation of H_3O_2^- IR spectra is a difficult task due to the high dimensionality of the problem and the floppy nature of the vibrational motion corresponding to proton transfer. Salahub et al.⁸ tested DFT molecular dynamics simulations with nonlocal functionals of GGA and LAP families. They found out that the geometry, calculated vibrational spectra of the hydroxide complexes (especially the vibrations involving the hydrogen bonds), and the dynamical proton-transfer counting autocorrelation function are very sensitive to the choice of the functional. Previous theoretical studies of *N*-methylacetamide in solution²⁴ have shown that the B3PW91 functional together with the 6-31G(d,p) basis set provides a computationally efficient way to calculate vibrational frequencies and intensities in good agreement with experimental data for the systems involving hydrogen bonding.

In this work, we present a detailed study of the IR spectrum of H_3O_2^- complex and its isotopomer D_3O_2^- using the MP2 computational level with the direct molecular dynamics approach at two temperatures, 100 and 300 K. To our knowledge, this is the first attempt to calculate the IR spectrum of this system at that level of theory. A comparison of our theoretical simulations to the experimental observations has been made, and the spectral features have been assigned using the normal-mode analysis (NMA), instantaneous normal mode (INM) analysis, isotopic substitution, polarized infrared absorptions, and analysis of the position–position correlation function. We performed a standard NMA²⁵ by diagonalizing the Hessian matrix at the equilibrium structure and obtained nine normal-mode frequencies and corresponding normal mode vectors for H_3O_2^- and D_3O_2^- . INM analysis was employed to predict the density of states and to attribute the spectral peaks to particular vibrational modes.

We also compared the results from MP2 and DFT (B3LYP, B3PW91) calculations to assess the accuracy and feasibility of the DFT approach to predict structure, vibrational frequencies, energetics, proton transfer barriers, proton population profile, and IR spectrum. The purpose of this work is to perform benchmark calculations using the direct molecular dynamics approach to obtain the IR spectra of H_3O_2^- and D_3O_2^- . This approach will make it possible to analyze the vibrational motion of larger hydrated ions, for which an analytical form of the potential energy and dipole surfaces is not available due to high dimensionality.

2. Computational Methods

All calculations were carried out using the second-order Møller–Plesset (MP2) perturbation theory,^{26–28} with the basis set augmented by *s* and *p* diffusion functions on the oxygen atoms only (denoted as cc-pVTZ(aug-O:s,p), and B3LYP^{29–31} and B3PW91^{31,32} methods with the 6-31+G(d,p) basis set. The geometry of the H_3O_2^- ground electronic state was optimized, and vibrational frequencies were obtained using the normal-mode analysis.

IR spectra of H_3O_2^- and D_3O_2^- were obtained by running direct molecular dynamics. The forces acting on the nuclei were computed from electronic structure calculations “on-the-fly” as the trajectory was generated at every time step. In this way, the construction of the explicit potential is avoided and the level of approximation in MD thus depends on the level of approximation for solving the Schrödinger equation, the choice of the method to calculate the potential energy and the basis set to describe the molecular orbitals. The direct molecular dynamics simulations were carried out on our Linux computer cluster using a shell script that interfaces the Gaussian 03 program³³ and our own suite of MD codes.

Spectra were collected for $J = 0$ using the expression for the intensity I

$$I(\omega) = \frac{Re}{\pi} \int_0^\infty dt e^{i\omega t} \langle \vec{\mu}(0) \cdot \vec{\mu}(t) \rangle_T \quad (1)$$

where ω is frequency and $\langle \vec{\mu}(0) \cdot \vec{\mu}(t) \rangle_T$ is the dipole–dipole correlation function at temperature T . Trajectories were propagated at a constant temperature via Berendsen’s thermostat.³⁴ The constant temperature was maintained with a 10 fs time response parameter.³⁴ The angular momentum was checked for conservation to ensure the accuracy of the propagator. The correlation function was then obtained as a time average along the trajectory.³⁵ Usually it is sufficient to run 10–20 long trajectories (order of picoseconds) to achieve convergence. For each temperature, the IR spectra were calculated from five trajectories propagated for 10 ps with a 0.5 fs time step (20 200 steps) at temperatures of 100 and 300 K using the B3LYP, B3PW91, and MP2 computational methods. We tested the convergence of the spectrum at the B3LYP level by running another five trajectories with different initial conditions. The shapes of the spectra from the two sets of simulations agree very well. The overlap of spectra from five and ten trajectories was 94% and 98% at 100 and 300 K, respectively. On the basis of this result, we concluded that five MP2 trajectories would yield a well-converged spectrum. The starting point for all trajectories was the equilibrium structure with randomly sampled velocities from the Boltzmann distribution. Initially the system was equilibrated for the first 200 steps. Then the IR spectrum was calculated by Fourier transform of dipole–dipole correlation function (eq 1), corrected with a quantum mechanical frequency-dependent factor.³⁶

The orientation of H_3O_2^- in the coordinate system and the atom labeling are shown in Figure 1. The *x*-axis is coincident with the OO-axis, the vibration of the shared proton between two oxygens. The IR spectra are plotted

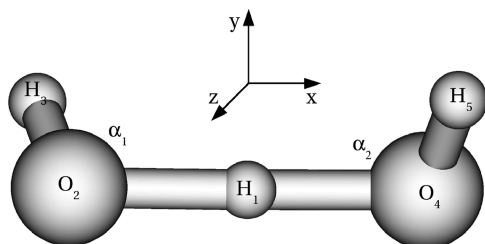


Figure 1. The orientation of H_3O_2^- in the coordinate system and the atom labeling.

separately for the parallel and perpendicular components, $\langle \mu_x(0)\mu_x(t) \rangle_T$ and $\langle \mu_y(0)\mu_y(t) + \mu_z(0)\mu_z(t) \rangle_T$, respectively. This separation of polarization into the parallel (along x -axis) and perpendicular (along y - and z -axes) components facilitates the spectral assignment of the peaks based on the internal movements.

We have also evaluated the classical position–position correlation function³⁵ from the coordinates saved along MD trajectories. The position–position correlation function was separated into the parallel (x -axis) and perpendicular (y - and z -axes) components

$$C_{\parallel} = \langle x(0)x(t) \rangle_T$$

$$C_{\perp} = \langle y(0)y(t) + z(0)z(t) \rangle_T \quad (2)$$

and the spectrum was obtained by Fourier transform.

In order to better interpret our classical MD spectra and to assess quantum and anharmonic effects in the H_3O_2^- system, an instantaneous normal-mode analysis^{37–40} was performed. We characterized the spectrum in a certain frequency window by calculating the overlap⁴¹ of the instantaneous normal mode vectors with the normal mode vectors of H_3O_2^- at the minimum

$$O_{jk} = \sum_{i=1}^{3N} x_{ik} u_{ij} \quad (3)$$

where u_j is the j th normal mode vector, and x_k is the instantaneous normal mode vector. The contribution of each normal mode to the normal mode of the instantaneous structure can be defined as an average weight²³

$$w_j = (1/N_f) \sum_{k=1}^{N_f} O_{jk}^2 \quad (4)$$

where N_f is the number of instantaneous structures in a given frequency window.

3. Results and Discussion

In this section, as a main result of this work, we present the IR spectra of H_3O_2^- and D_3O_2^- calculated using MP2/cc-pVTZ(aug-O:s,p) direct MD simulations. The geometry was optimized at the MP2 level of theory to a nonplanar structure with an asymmetric hydrogen bond. The structural parameters are listed in Table 1 and the labeling of the atoms is shown in Figure 1. The geometrical parameters for MP2/cc-pVTZ(aug-O: s,p) structure are in close agreement to those predicted by Xantheas² at the MP2/aug-cc-pVTZ level of

Table 1. H_3O_2^- Minimum Structure Using B3LYP, B3PW91, and MP2 Methods

internal coordinates ^a	B3LYP	B3PW91	MP2
R_1 ($\text{O}_2\text{--H}_1$), Å	1.309	1.222	1.331
R_2 ($\text{O}_4\text{--H}_1$), Å	1.154	1.222	1.130
R_3 ($\text{O}_2\text{--H}_3$), Å	0.966	0.963	0.962
R_4 ($\text{O}_4\text{--H}_5$), Å	0.965	0.963	0.960
α_1 ($\text{H}_1\text{--O}_2\text{--H}_3$), deg	106.5	104.5	103.5
α_2 ($\text{H}_1\text{--O}_4\text{--H}_5$), deg	103.8	104.5	101.7
δ_1 ($\text{O}_2\text{--H}_1\text{--O}_4\text{--H}_5$), deg	177.8	179.0	178.1
δ_2 ($\text{H}_3\text{--O}_2\text{--O}_4\text{--H}_5$), deg	110.5	111.0	106.8

^a The labeling of the atoms is shown in the Figure 1.

Table 2. H_3O_2^- and D_3O_2^- Normal Mode Frequencies in cm^{-1} Using B3LYP, B3PW91, and MP2 Methods

	B3LYP		B3PW91		MP2	
	H_3O_2^-	D_3O_2^-	H_3O_2^-	D_3O_2^-	H_3O_2^-	D_3O_2^-
OH torsion	200	146	199	145	199	145
OO stretch	276	216	575	428	310	259
OH wag	515	416	225	160	519	404
OH rock	594	433	634	613	610	440
BH stretch, x -axis	967	790	631	465	1120	894
BH bend, z -axis	1446	1041	1489	1073	1433	1031
BH bend, y -axis	1672	1206	1668	1203	1686	1215
OH stretch	3825	2784	3872	2818	3864	2812
OH stretch	3844	2797	3873	2818	3890	2830

theory. In our work, we have chosen truncated basis set cc-pVTZ(aug-O:s,p) to save computational time when running MP2 molecular dynamics simulations. Sauer and Dobler⁴² calculated gas-phase IR spectra for hydrated water dimer H_5O_2^+ using MP2. They showed that the MP2/aug-cc-pVTZ and MP2/cc-pVTZ(aug-O) harmonic frequencies were very similar and concluded that the truncated basis set provides accurate $\text{O--H}^+\cdots\text{O}$ asymmetric stretch frequency.

A. Dipole Spectra. The assignment of the spectral peaks was made by comparing our MP2 IR spectra and recent experimental IR spectra^{16,21} to the previous high level calculations^{14,15} and normal-mode frequencies listed in Table 2. Figure 2 illustrates the IR spectrum of the H_3O_2^- calculated using MP2 at 100 and 300 K. The most dominant peak in our MP2 spectrum at 100 K (Figure 2a) centered at 250 cm^{-1} can be assigned to the OH torsional motion. Now we aim to investigate the spectral region associated with the motion of the shared proton in H_3O_2^- . The experimental argon predissociation spectrum (see Figure 2b in ref 21) exhibits a dominant spectral feature at 697 cm^{-1} and two small peaks around 1000 cm^{-1} assigned to bridging hydrogen (BH) motion (motion of a proton between the two oxygens) parallel and perpendicular to the hydrogen-bond axis, respectively. Another experimental study of the intramolecular bending transitions in the $1000\text{--}1900\text{ cm}^{-1}$ region¹⁶ identifies the spectral feature near 1090 cm^{-1} as excitation of the shared proton along and/or perpendicular to the O–O axis¹⁵ based on diffusion Monte Carlo¹⁶ and the VSCF/CI methods.¹⁴ Our MP2 spectrum in the region between 400 and 1800 cm^{-1} (Figure 2b) shows a broad feature between 500 and 1200 cm^{-1} with dominant peaks between 500 and 800 cm^{-1} , while the experimental spectrum²¹ predicts a relatively narrow absorption peak at 697 cm^{-1} with Δ_{fwhm}

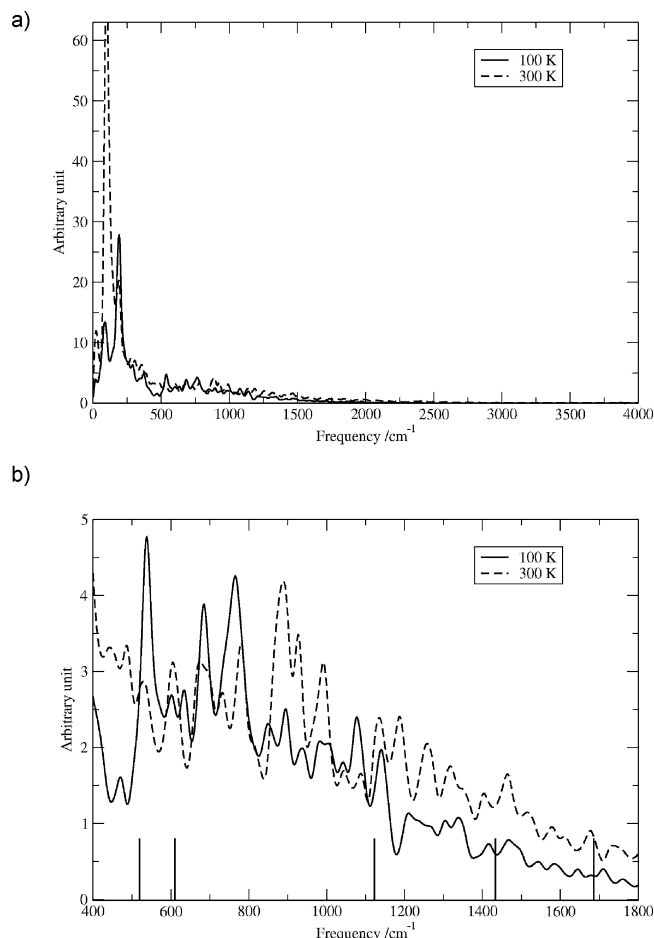


Figure 2. MD MP2 IR spectra for H_3O_2^- at 100 and 300 K (a) in the full spectral range and (b) in the range from 400 to 1800 cm^{-1} . The harmonic frequencies are shown as sticks in the spectrum.

$= 21 \text{ cm}^{-1}$. Simulations at 300 K show that this spectral feature broadens significantly.

The quantum studies of the in H_3O_2^- and D_3O_2^- vibrations^{14,15} assigned the spectral bands between 500 and 800 cm^{-1} to the OO stretch, OH wagging, OH rocking, and BH stretch modes. Normal mode analysis predicts large x displacements for these vibrations. BH stretch parallel to the hydrogen-bond axis (x -axis in our case) is the most effective for modulation of the molecular dipole; therefore, it should have the stronger intensity in the spectrum. Our H_3O_2^- and D_3O_2^- IR spectra calculated at the MP2 level at 100 K (Figure 3) show that the parallel components of the dipole–dipole correlation function contribute significantly to the total spectral intensity, while contributions from the perpendicular components are much smaller. In the spectral range between 500 and 800 cm^{-1} , the MP2 IR spectrum of H_3O_2^- calculated with only the parallel component of the dipole–dipole correlation function (Figure 3a) shows three infrared bands with similar intensities at 540, 685, and 765 cm^{-1} and two small peaks at 1075 and 1140 cm^{-1} . When the IR spectrum is calculated only with perpendicular components of the dipole–dipole correlation function (Figure 3b), peaks at 685, 765, 1075, and 1140 cm^{-1} disappear, and we can conclude that character of these spectral peaks correspond to modes with large displacements along the

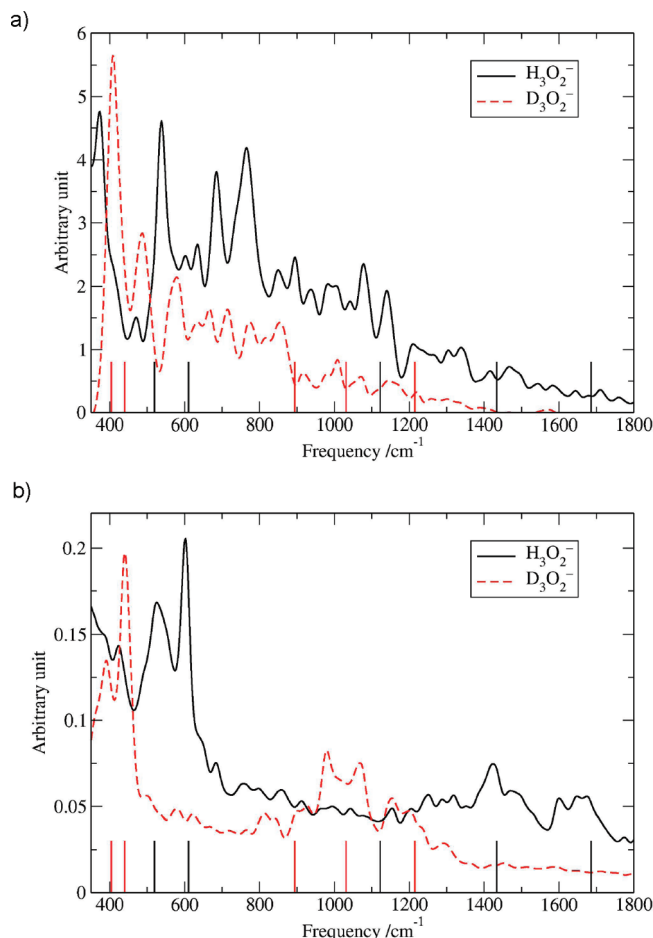


Figure 3. MD MP2 IR spectra at 100 K for H_3O_2^- and D_3O_2^- calculated using the dipole–dipole correlation function decomposed to (a) the parallel $\langle \mu_x(0)\mu_x(t) \rangle_T$ and (b) perpendicular $\langle \mu_y(0)\mu_y(t) + \mu_z(0)\mu_z(t) \rangle_T$ components. The harmonic frequencies are shown as sticks in the spectrum.

x -axis (e.g., OO stretch, OH wagging, OH rocking, or BH stretch). We will later confirm these assignments using the position–position correlation function and INM analysis (see below).

Normal mode analysis predicts two BH bend modes at 1433 and 1686 cm^{-1} at the MP2 level. Quantum studies¹⁵ place these modes between 1300 and 1500 cm^{-1} . Our MP2 spectrum (Figure 2b) does not show distinct spectral peaks in this region. However, when MP2 IR intensities are calculated using the perpendicular component of the dipole–dipole correlation function, BH bend modes can be found in the spectrum at 1450 and 1650 cm^{-1} (Figure 3b). Both spectral peaks shift by about 450 cm^{-1} upon isotopic substitution.

B. Position–Position Spectra. In order to address the issue with the many overlapping features in the IR spectrum shown in the Figure 2b, we calculated a few representative position–position spectra from the coordinates saved along MP2 trajectory at 100 K. Figure 4 shows the total intensities and the parallel and perpendicular components along the x - and yz -directions, respectively, for the terminal hydrogens, bridging hydrogen, and for OO-stretch position vectors. The placement of the peaks in the position–position spectra can be directly compared to the placement of peaks in the IR

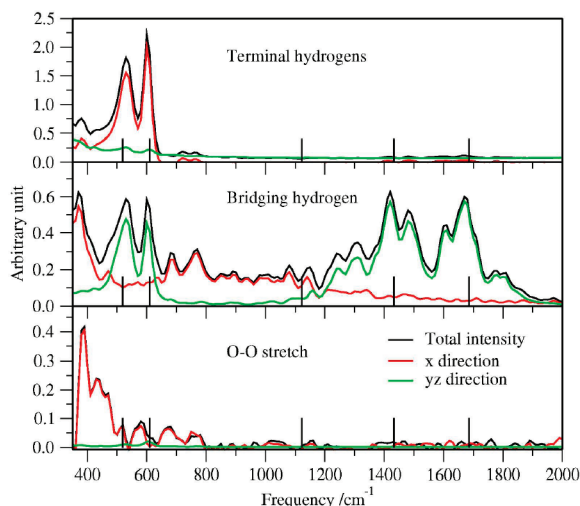


Figure 4. The MP2 vibrational spectrum at 100 K obtained by Fourier transform of the position–position correlation function. The spectrum was decomposed into the contributions from the terminal hydrogens H3 and H5 (top panel), bridging hydrogen H1 (middle panel), and OO stretch position vectors (bottom panel). This figure shows the total intensities (black lines) and the parallel (red lines) and perpendicular components (green lines) along the *x*- and *yz*-directions, respectively.

spectra (Figure 2b). However, the intensity of the peaks should not be compared directly, because a position–position spectrum does not reflect dipole activity.

The position–position spectra clearly identify the activity of OH wag, OH rock, OO stretch, BH parallel, and perpendicular vibrations. We note that the base lines of these spectra are well-defined. Our MD simulations predict the OO stretch vibration to be blue-shifted by about 90 cm^{-1} . The position–position spectrum is showing the OO stretch peak at 400 cm^{-1} , while the harmonic frequency is 310 cm^{-1} . The terminal hydrogens exhibit activity in the spectral region from 400 to 2000 cm^{-1} for OH wag and OH rock vibrations, as expected from the normal-mode analysis. The position–position spectrum of the bridging hydrogen is more complex, clearly showing regions where the parallel (along *x*-axis) and perpendicular (along *y*- and *z*-axes) components dominate. BH perpendicular component is showing two doublets near two bending harmonic vibrations at 1433 and 1686 cm^{-1} and two weak features at 1250 and 1300 cm^{-1} . The BH perpendicular component is also strongly coupled to both OH wag and OH rock vibrations at 519 and 610 cm^{-1} , respectively.

The BH mode exhibits large displacements along the O–O axis (*x*-axis) up to 1200 cm^{-1} . The harmonic frequency for BH stretch along the *x* axis is 1120 cm^{-1} (Table 1). The baseline of the position–position spectrum of parallel components is not as well-defined as that of the perpendicular component. There is a strong peak at 400 cm^{-1} that coincides with the O–O stretch and four weak features at 700, 780, 1080, and 1140 cm^{-1} that are most likely combination bands of BH stretch and other modes. This analysis of the position–position spectra brings new insights into understanding the complexity of the IR spectrum shown in Figure 2b).

Comparison of the MP2 and experimental spectra demonstrates that MP2 is capturing the essential spectral feature of the BH stretch mode between 600 and 900 cm^{-1} . The main difference between our MP2 spectrum and experimental spectra^{16,21} lies in the observation of the feature near 1090 cm^{-1} . Quantum studies^{15,16} reveal large displacements of the shared proton along and/or perpendicular to the O–O axis in the 1000–1100 cm^{-1} region. From the analysis of our IR spectrum using the polarized dipole absorptions and position–position correlation function, we can conclude that these spectral features most likely originate from the parallel motion of the shared proton coupled to other modes (Figure 2). Our results predict the perpendicular motion of the shared proton between 1250 and 1650 cm^{-1} (Figure 4).

C. Comparison of Methods. We also examined how B3LYP and B3PW91 methods perform for this system. The DFT and MP2 structural parameters, potential energy features, the results from the direct MD simulations, and interpretation of the trajectories were compared with the aim of assessing the reliability of DFT functionals for this anion. The B3LYP and B3PW91 structural parameters are listed in the Table 1. The geometry optimized at the B3LYP level of theory shows a nonplanar structure with an asymmetric hydrogen bond, while the B3PW91 calculations failed to reproduce the asymmetry of the hydrogen bond in H_3O_2^- . If the larger basis set 6-311++G(2d,2p) is used, H_3O_2^- remains nearly symmetrical with R_1 and R_2 distances equal to 1.227 and 1.214 Å, respectively. Harmonic vibrational frequencies for H_3O_2^- and D_3O_2^- are listed in the Table 2. B3LYP and MP2 vibrational frequencies are in very good agreement. The largest differences appear in the BH modes. BH stretch frequencies along the *x* axis are 967 and 1120 cm^{-1} at B3LYP and MP2 levels, respectively. The bridging hydrogen motion is a large amplitude mode with normal mode displacement values above 0.8. The BH stretch frequency is sensitive to the shape of the potential near the transition state for the proton transfer. The normal mode assignment for B3PW91 differs from the B3LYP and MP2 mode assignment because B3PW91 failed to reproduce the asymmetry of the hydrogen bond in H_3O_2^- . In the B3LYP and MP2 case, the OH stretch frequencies are localized on either of the OH bonds, while in the B3PW91 case, OH stretch frequencies are assigned as symmetric and asymmetric OH stretch.

The proton motion between the two oxygens in H_3O_2^- is characterized by a 74 cm^{-1} barrier on the potential energy surface calculated at CCSD(T) computational level.¹⁴ MP2 and B3LYP calculations predict much lower barrier heights about 13 and 5 cm^{-1} , respectively, and H_3O_2^- experiences no energy barrier at the B3PW91 level. The qualitative differences between the potentials calculated at DFT and MP2 levels are further analyzed in terms of the potential energy surface scanned along the normal mode displacements. Figure 5a shows potential energy curves along the BH stretch and O–H stretch normal mode displacements. The shapes of the potential energy curves are almost identical for B3LYP and MP2 calculations, while at the B3PW91 level the potential is much more flat at displacements beyond 0.6 Å. Figure 5b depicts the

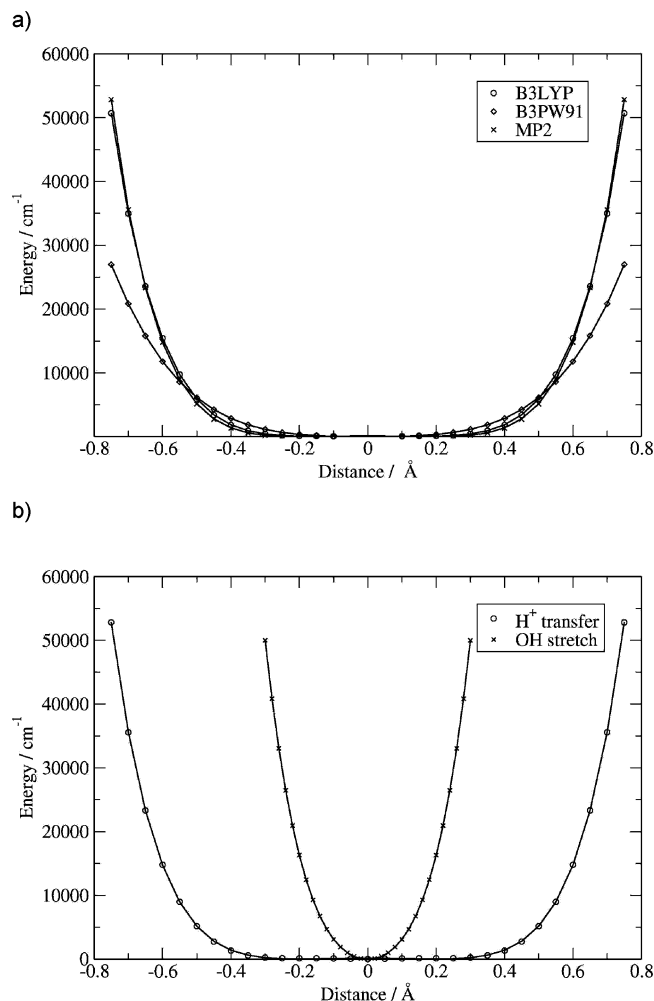


Figure 5. Potential energy curves along (a) the H^+ transfer (BH stretch along x -axis) normal mode displacements calculated by B3LYP, B3PW91, and MP2 methods. (b) H^+ transfer and O-H stretch normal mode displacements calculated by the MP2 method.

floppiness of molecular motion along the BH stretch normal mode displacement compared to the OH stretch mode at the MP2 level of theory.

The bond-length distributions for a proton transfer averaged over five direct MD trajectories calculated by B3LYP, B3PW91, and MP2 methods are shown in Figure 6. It is apparent that difference in the potential energy surface near the transition state for the proton transfer in H_3O_2^- influences the dynamical behavior of the system. At B3LYP and MP2 levels the bond-length distributions are broad and show two peaks, while at the B3PW91 level it is much narrower due to the absence of the barrier for the proton transfer.

Figure 7 presents a comparison of the simulated IR spectra up to 2000 cm^{-1} calculated at 100 K by B3LYP, B3PW91, and MP2 methods. The spectral intensities from MP2 and B3LYP calculations are very similar, while B3PW91 predicts different spectral intensities due to the qualitative differences in the potential energy and dipole moment surfaces.

D. Temperature Dependence of the B3LYP Spectra. Since it is not entirely clear from the experiment²¹ at which temperature the spectrum was measured, we performed a

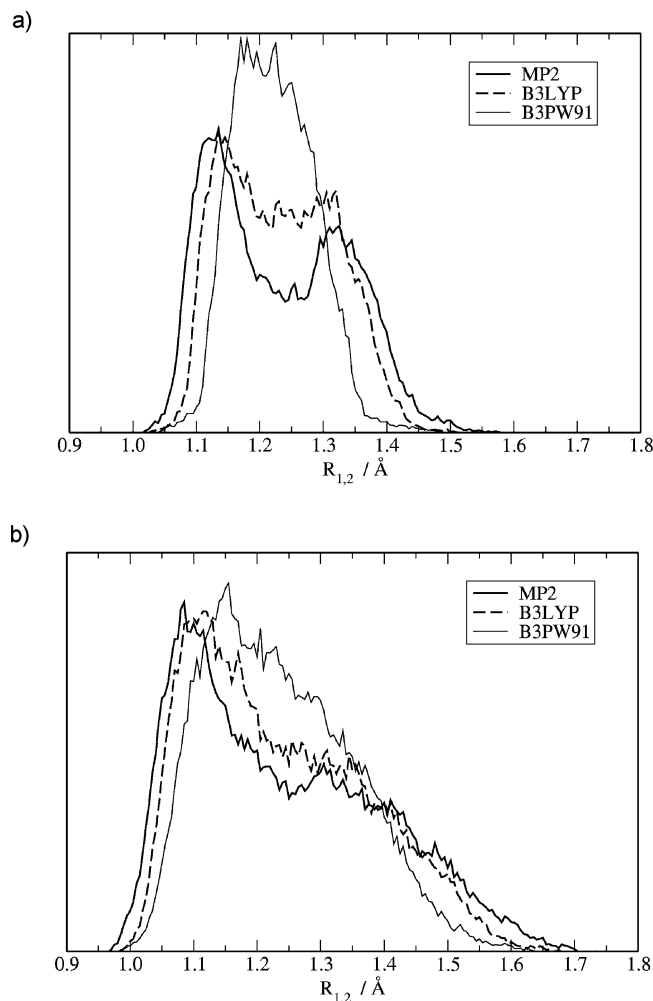


Figure 6. Bond-length distributions for H^+ transfer according to MD B3LYP, B3PW91, and MP2 calculations at (a) 100 K and (b) 300 K.

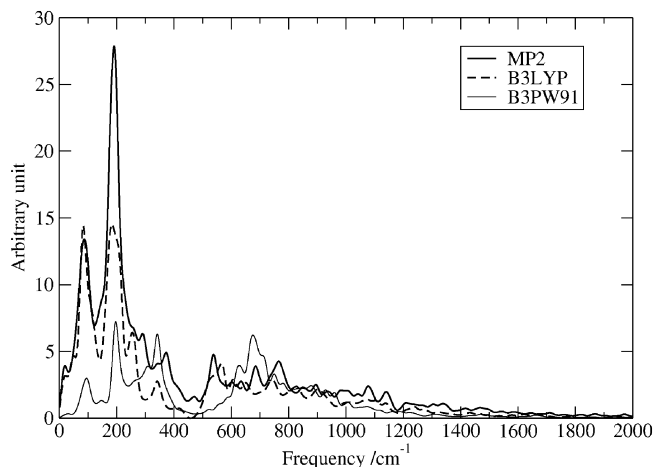


Figure 7. Comparison of MD B3LYP, B3PW91, and MP2 IR spectra for H_3O_2^- at 100 K.

series of calculations to try to determine experimental conditions. In Figure 8 we show the temperature dependence of the B3LYP spectra from 10 to 300 K. At 10 K the B3LYP spectrum is essentially harmonic. Only the BH stretch vibration along the x -axis is red-shifted by about 50 cm^{-1} . At 50 K the spectrum is starting to show a significant

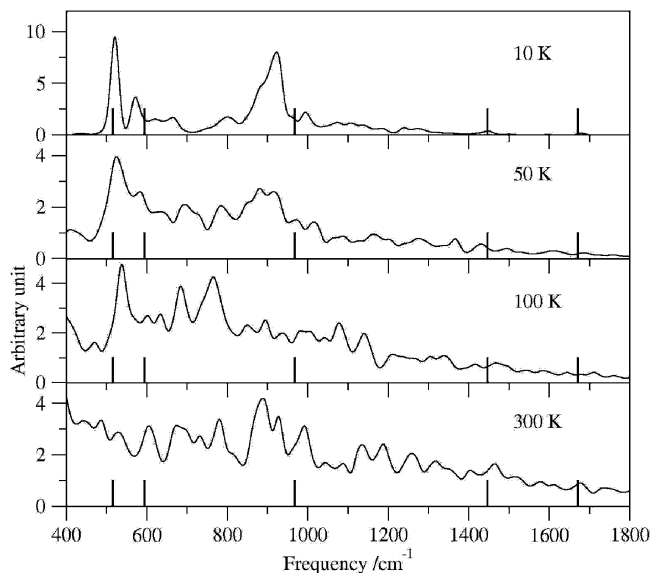


Figure 8. Temperature dependence of the B3LYP spectra from 10 to 300 K. The IR spectra were obtained from 10 trajectories propagated for 10 ps. The harmonic frequencies are shown as sticks in the spectrum.

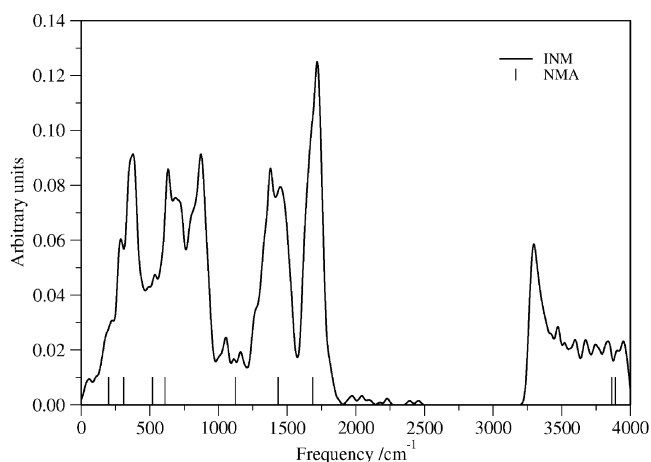


Figure 9. Vibrational density of states obtained from INM analysis of MP2 MD simulations at 100 K. The harmonic frequencies are shown as sticks in the spectrum.

temperature effect. One can see new peaks arising between 600 and 900 cm^{-1} that originate from coupling of the BH with other modes, as we have mentioned above. This trend continues at higher temperature, where there is also much more activity above 1000 cm^{-1} . On the basis of these observations we believe that the experimental spectrum²¹ was measured at a relatively low temperature, possibly <50 K.

E. INM Spectra. The INM spectrum was obtained by calculating the INM frequencies for 500 instantaneous configurations drawn from the course of a direct MD simulations at the MP2 level at temperature 100 K. Because the system is not at its global potential energy minimum, some modes represent unstable motions, and these unstable modes have imaginary frequencies, which are omitted in the analysis. Figure 9 shows the INM density of states in the range from 0 to 4000 cm^{-1} for H_3O_2^- . The normal-mode frequencies are shown as sticks in the spectrum. In this figure we can see broad bands peaking at 375, 630, 870, 1400, and

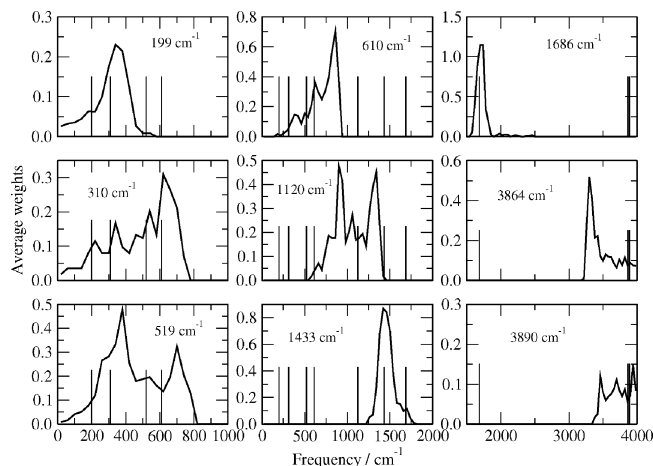


Figure 10. Average weights representing the overlap of the MP2 instantaneous normal mode vectors and the normal mode vectors calculated at the H_3O_2^- minimum structure. The harmonic frequencies are shown as sticks in the spectrum.

1720 cm^{-1} . The peak positions of the density of states can be identified as normal-mode frequencies at 310, 610, 1433, and 1686 cm^{-1} . However, there is no normal mode in the spectral region between 610 and 1120 cm^{-1} ; therefore, we assume that the peak at 870 cm^{-1} is either a combination band or a strongly shifted fundamental. Instantaneous normal modes for OH stretch motion are red-shifted with the maximum peak at 3300 cm^{-1} . MP2 MD simulations predict two weak OH stretch frequencies at 3685 and 3880 cm^{-1} for H_3O_2^- and 2660 and 2820 cm^{-1} for D_3O_2^- . However, the position of the peaks are not thought to be reliable because of the relatively long propagation time step.

Figure 10 shows average weights for all nine H_3O_2^- normal modes. The peaks in the spectral regions around 1400 and 1700 cm^{-1} are relatively narrow. We conclude that the instantaneous modes in these spectral windows overlap with normal modes at 1433 and 1686 cm^{-1} , respectively. Instantaneous normal modes up to 800 cm^{-1} overlap with several low frequency normal modes, showing blue and red anharmonic shifts. BH stretch normal mode at 1120 cm^{-1} overlaps with instantaneous normal modes in the range from 700 to 1400 cm^{-1} showing maximum overlaps at 900 and 1340 cm^{-1} . Experimentally, BH stretch was observed at 697 cm^{-1} .²¹ The character of the broad spectral feature in the INM density of states (Figure 9) near 870 cm^{-1} can be assigned to the combination of the OH rock vibration (75%) and BH stretch vibration along the x -axis (25%). The assignment of this frequency is in agreement with the assignment of the IR spectrum obtained from our direct MD simulations.

INM analysis that we carried out in this work is temperature-dependent, because the instantaneous structures were sampled from MD trajectories propagated at fixed temperature. At very low temperature, MD trajectories sample structures that are very similar to the minimum on the potential energy surface, while at higher temperature, multiple minima can be visited; therefore, the instantaneous normal mode spectrum could be regarded as a weighted average over several minima. In such a case, overlaps of normal mode vectors for instantaneous struc-

tures with other minima can be weighted by a factor that reflects the distance of an instantaneous structure from that minimum, i.e., $1/|\vec{r}^{\text{MIN}} - \vec{r}^{\text{INM}}|^2$. We plan to use this approach for studying larger, more floppy water clusters.

4. Conclusions

In this work, we present IR spectra of H_3O_2^- and its isotopomer D_3O_2^- using the MP2, B3LYP, and B3PW91 direct molecular dynamics simulations. Despite some qualitative differences in the interaction potentials between B3PW91 and MP2 levels, the spectral patterns were found to be in reasonable agreement. IR spectra generated by B3LYP and MP2 methods show a qualitatively similar picture as those obtained from experimental studies.^{16,21} We assigned the spectral peaks in our classical IR spectrum calculated at the MP2 computational level at 100 K using INM analysis, by decomposition the IR spectral intensities into the parallel and perpendicular components, and by analysis of the position–position correlation function. Our results predict the bridging hydrogen stretch between 600 and 900 cm^{-1} and bridging hydrogen bend vibrations between 1250 and 1650 cm^{-1} . On the basis of our temperature-dependence study of the B3LYP spectrum, we believe that the experimental spectrum²¹ was measured at a very low temperature.

With this study, we hope that we have presented convincing evidence that the B3LYP method provides an accurate description of the interaction potential and dipole surfaces and can be used in simulations of larger hydrated ions. For more concrete assignment of spectral features, we plan to carry out driven MD simulations.^{23,43} Spectra will be analyzed using the method shown in ref 23.

Acknowledgment. We thank the Research Corp. for support of this work, Kennesaw State University for support under Faculty Summer Research Award, Incentive Funding Awards. We also thank Prof. J. M. Bowman (Emory University, Atlanta, GA) and Prof. M. B. Mitchell (Kennesaw State University) for many useful discussions on this project.

References

- Nagle, J. F. *J. Bioenerg. Biomembr.* **1987**, *19*, 413–426.
- Xantheas, S. S. *J. Am. Chem. Soc.* **1995**, *117*, 10373–10380.
- Tuckerman, M. E.; Marx, D.; Klein, M. L.; Parrinello, M. *Science* **1997**, *275*, 817–820.
- Tunon, I.; Martins-Costa, M. T. C.; Millot, C.; Ruiz-Lopez, M. F. *J. Chem. Phys.* **1997**, *106*, 3633–3642.
- Perez del Valle, C.; Novoa, J. J. *Chem. Phys. Lett.* **1997**, *269*, 401–407.
- Ruiz-Lopez, M. F.; Oliva, A.; Bertran, J. *J. Phys. Chem.* **1998**, *102*, 10728–10735.
- Turki, N.; Milet, A.; Rahmouni, A.; Ouamerali, O.; Moszynski, R.; Kochanski, E.; Wormer, P. E. S. *J. Chem. Phys.* **1998**, *109*, 7157–7168.
- Wei, D.; Proynov, E. I.; Milet, A.; Salahub, D. R. *J. Phys. Chem. A* **2000**, *104*, 2384–2395.
- Barich, D. H.; Nicholas, J. B.; Haw, J. F. *J. Phys. Chem. A* **2001**, *105*, 4708–4715.
- Chaudhuri, C.; Wang, Y. S.; Jiang, J. C.; Lee, Y. T.; Chang, H. C.; Nieder-Schatteburg, G. *Mol. Phys.* **2001**, *99*, 1161–1173.
- Samson, C. C. M.; Klopper, W. *J. Mol. Struct. (THEOCHEM)* **2002**, *586*, 201–208.
- Tuckerman, M. E.; Marx, D.; Parrinello, M. *Nature* **2002**, *417*, 926–929.
- Yeh, L. I.; Okumura, M.; Meyers, J. D.; Price, J. M.; Lee, Y. T. *J. Chem. Phys.* **1989**, *91*, 7319–7330.
- Huang, X.; Braams, B. J.; Carter, S.; Bowman, J. M. *J. Am. Chem. Soc.* **2004**, *126*, 5042–5043.
- McCoy, A. B.; Huang, X.; Carter, S.; Bowman, J. M. *J. Chem. Phys.* **2005**, *123*, 064317–064330.
- Diken, E. G.; Headrick, J. M.; Roscioli, J. R.; Bopp, J. C.; Johnson, M. A.; McCoy, A. B.; Huang, X.; Carter, S.; Bowman, J. M. *J. Phys. Chem. A* **2005**, *109*, 571–575.
- Teige, V. E.; Li, X.; Iyengar, S. S. *J. Phys. Chem. A* **2007**, *111*, 4815–4820.
- Yang, Y.; Kuhn, O. Z. *Phys. Chem.* **2008**, *222*, 1375–1387.
- Price, E. A.; Robertson, W. H.; Diken, E. G.; Weddle, G. H.; Johnson, M. A. *Chem. Phys. Lett.* **2002**, *366*, 412–416.
- Robertson, W. H.; Diken, E. G.; Price, E. A.; Shin, J. W.; Johnson, M. A. *Science* **2003**, *299*, 1367–1372.
- Diken, E. G.; Headrick, J. M.; Roscioli, J. R.; Bopp, J. C.; Johnson, M. A.; McCoy, A. B. *J. Phys. Chem. A* **2005**, *109*, 1487–1490.
- Hammer, N. I.; Diken, E. G.; Headrick, J. M.; Roscioli, J. R.; Johnson, M. A.; Myshakin, E. M.; Jordan, K. D.; McCoy, A. B.; Huang, X.; Bowman, J. M.; Carter, S. *J. Chem. Phys.* **2005**, *122*, 244301–244310.
- Kaledin, M.; Kaledin, A. L.; Bowman, J. M. *J. Phys. Chem. A* **2006**, *110*, 2933–2939.
- Kubelka, J.; Keiderling, T. A. *J. Phys. Chem. A* **2001**, *105*, 10922–10928.
- Wilson, E. B.; Decius, J. C.; Cross, P. C. *Molecular Vibrations*; McGraw-Hill: New York, 1955.
- Head-Gordon, M.; Pople, J. A.; Frisch, M. J. *Chem. Phys. Lett.* **1988**, *153*, 503–506.
- Saebo, M. J. S.; Almlöf, J. *Chem. Phys. Lett.* **1989**, *154*, 83–89.
- Frisch, M. J.; Head-Gordon, M.; Pople, J. A. *Chem. Phys. Lett.* **1990**, *166*, 275–280.
- Lee, C.; Yang, W.; Parr, R. G. *Phys. Rev. B* **1988**, *37*, 785–789.
- Becke, A. D. *J. Chem. Phys.* **1993**, *98*, 1372–1377.
- Becke, A. D. *J. Chem. Phys.* **1993**, *98*, 5648–5652.
- Perdew, J. P.; Wang, Y. *Phys. Rev. B* **1992**, *45*, 13244–13249.
- Frisch, M. J.; Trucks, G. W.; Schlegel, H. B.; Scuseria, G. E.; Robb, M. A.; Cheeseman, J. R.; Montgomery, J. A., Jr.; Vreven, T.; Kudin, K. N.; Burant, J. C.; Millam, J. M.; Iyengar, S. S.; Tomasi, J.; Barone, V.; Mennucci, B.; Cossi, M.; Scalmani, G.; Rega, N.; Petersson, G. A.; Nakatsuji, H.; Hada, M.; Ehara, M.; Toyota, K.; Fukuda, R.; Hasegawa, J.; Ishida, M.; Nakajima, T.; Honda, Y.; Kitao, O.; Nakai, H.; Klene, M.; Li, X.; Knox, J. E.; Hratchian, H. P.; Cross, J. B.; Bakken, V.; Adamo, C.; Jaramillo, J.; Gomperts, R.; Stratmann, R. E.; Yazyev, O.; Austin, A. J.; Cammi, R.; Pomelli, C.; Ochterski, J. W.; Ayala, P. Y.; Morokuma, K.; Voth, G. A.; Salvador, P.; Dannenberg, J. J.

- Zakrzewski, V. G.; Dapprich, S.; Daniels, A. D.; Strain, M. C.; Farkas, O.; Malick, D. K.; Rabuck, A. D.; Raghavachari, K.; Foresman, J. B.; Ortiz, J. V.; Cui, Q.; Baboul, A. G.; Clifford, S.; Cioslowski, J.; Stefanov, B. B.; Liu, G.; Liashenko, A.; Piskorz, P.; Komaromi, I.; Martin, R. L.; Fox, D. J.; Keith, T.; Al-Laham, M. A.; Peng, C. Y.; Nanayakkara, A.; Challacombe, M.; Gill, P. M. W.; Johnson, B.; Chen, W.; Wong, M. W.; Gonzalez, C.; Pople, J. A. *Gaussian 03, Revision C.02*; Gaussian, Inc.: Wallingford, CT, 2004.
- (34) Berendsen, H. J. C.; Postma, J. P. M.; Van Gunsteren, W. F.; Dinola, A.; Haak, J. R. *J. Chem. Phys.* **1984**, *81*, 3684–3690.
- (35) Haile, J. M. *Molecular Dynamics Simulation: Elementary Methods*; Wiley & Sons: New York, 1992; p 277.
- (36) Berens, P. H.; Wilson, K. R. *J. Chem. Phys.* **1981**, *74*, 4872–4882.
- (37) Stratt, R. M. *Acc. Chem. Res.* **1995**, *28*, 201–207.
- (38) Keyes, T. *J. Chem. Phys.* **1996**, *104*, 9349–9356.
- (39) Buchner, M.; Ladanyi, B. M.; Stratt, R. M. *J. Chem. Phys.* **1992**, *97*, 8522–8535.
- (40) Cho, M.; Fleming, G. R.; Saito, S.; Ohmine, I.; Stratt, R. M. *J. Chem. Phys.* **1994**, *100*, 6672–6683.
- (41) Li, X.; Moore, D. T.; Iyengar, S. S. *J. Chem. Phys.* **2008**, *128*, 184308.
- (42) Sauer, J.; Dobler, J. *ChemPhysChem* **2005**, *6*, 1706–1710.
- (43) Bowman, J. M.; Zhang, X.; Brown, A. *J. Chem. Phys.* **2003**, *119*, 646–650.

CT8004485